Schistosoma mansoni Fatty Acid Binding Protein: Specificity and Functional Control as Revealed by Crystallographic Structure[†,‡]

Francesco Angelucci,[§] Kenneth A. Johnson,[§] Paola Baiocco,[§] Adriana E. Miele,[§] Maurizio Brunori,[§] Cristiana Valle,[||] Fabio Vigorosi,[||] Anna Rita Troiani,[||] Piero Liberti,[||] Donato Cioli,[||] Mo-Quen Klinkert,[⊥] and Andrea Bellelli*[,§]

Department of Biochemical Sciences "A. Rossi Fanelli", CNR Institute of Molecular Biology and Pathology and Istituto Pasteur-Fondazione Cenci Bolognetti, University of Rome "La Sapienza", Piazzale Aldo Moro 5, 00185 Rome, Italy, CNR Institute of Cell Biology, 32 Via Ramarini, 00016 Monterotondo, Rome, Italy, and Bernhard-Nocht-Institut für Tropenmedizin, 74 Bernhard-Nocht-Strasse, 20359 Hamburg, Germany

Received July 14, 2004

ABSTRACT: *Schistosoma mansoni* fatty acid binding protein (Sm14) was crystallized with bound oleic acid (OLA) and arachidonic acid (ACD), and their structures were solved at 1.85 and 2.4 Å resolution, respectively. Sm14 is a vaccine target for schistosomiasis, the second most prevalent parasitic disease in humans. The parasite is unable to synthesize fatty acids depending on the host for these nutrients. Moreover, arachidonic acid (ACD) is required to synthesize prostaglandins employed by schistosomes to evade the host's immune defenses. In the complex, the hydrocarbon tail of bound OLA assumes two conformations, whereas ACD adopts a unique hairpin-looped structure. ACD establishes more specific interactions with the protein, among which the most important is a π-cation bond between Arg78 and the double bond at C8. Comparison with homologous fatty acid binding proteins suggests that the binding site of Sm14 is optimized to fit ACD. To test the functional implications of our structural data, the affinity of Sm14 for 1,8-anilinonaphthalenesulfonic acid (ANS) has been measured; moreover the binding constants of six different fatty acids were determined from their ability to displace ANS. OLA and ACD exhibited the highest affinities. To determine the rates of fatty acid binding and dissociation we carried out stopped flow kinetic experiments monitoring displacement by (and of) ANS. The binding rate constant of ligands is controlled by a slow pH dependent conformational change, which we propose to have physiological relevance.

Schistosomiasis is the second most prevalent parasitic disease worldwide and affects more than 200 million people in developing countries. Schistosomes are parasitic trematodes whose complex life cycle involves an intermediate host (a freshwater snail) and man as the definitive host. Adult schistosomes live in the mesenteric or perivesical veins of their definitive host and uptake their nutrients directly from the host's blood.

The proteins that participate in the uptake and metabolism of fatty acids and their derivatives may constitute a possible target for therapy or vaccination, given the numerous and important roles played by these compounds. To briefly review this subject, we remark that the parasite lacks the metabolic pathways required for the biosynthesis of sterols and lipids; hence it is completely dependent on the host for these substances (*1*). Besides being nutrients and structural components of the cell membrane, fatty acid derivatives released by schistosomes play a role in the parasite evasion from the host immune response (*2*). Moreover, upon contact with human skin, cercariae (the larval stage released by the intermediate host) respond to chemical stimuli, particularly medium-chain free fatty acids, to start skin invasion (*3*). Uptake and transport of fatty acids and other lipids in *S. mansoni* depend (probably to a large extent) on the fatty acid binding protein (Sm14)[1] (*4*). Sm14 is present in all the stages of the life cycle and is localized in the external cell layer, i.e., near the interface of the parasite/host contact (*5*). From this short summary an important conclusion may be drawn: interfering with fatty acid uptake or metabolism may constitute an important therapeutical approach. Accordingly, the World Health Organization selected Sm14 as one out of six antischistosome vaccine candidates for testing (*6*, *7*); and possibly the protein may also be a drug target, since blocking of fatty acid uptake could have dramatic effects on the life

[†] Funding was received by the University of Rome "La Sapienza" (Progetto Ateneo 60%—anno 2003) and by the Ministero dell'Università e della Ricerca Scientifica e Tecnologica of Italy (PRIN 2003). Elettra (Trieste, Italy) provided generous fellowships to K.A.J. and P.B.

[‡] Sm14−ACD and Sm14−OLA have been deposited with PDB codes 1VYF and 1VYG, respectively.

* To whom correspondence should be addressed. Tel: +39 06499 10236. Fax: +39 06444 0062. E-mail: andrea.bellelli@uniroma1.it.

[§] University of Rome "La Sapienza".

[||] CNR Institute of Cell Biology.

[⊥] Bernhard-Nocht-Institut für Tropenmedizin.

[1] Abbreviations: FABP, fatty acid binding protein; Sm14, *Schistosoma mansoni* FABP; SjFABP, *Schistosoma japonicum* FABP; Eg-FABP1, *Echinococcus granulosus* FABP; I-FABP, intestinal FABP; H-FABP, heart/muscle FABP; A-FABP, adipocyte FABP; B-FABP, brain FABP; M-FABP, myelin P2 FABP; L-FABP, liver FABP; CMC, critical micellar concentration; FA, fatty acid; OLA, oleic acid; ACD, arachidonic acid; LA, linoleic acid; PA, palmitic acid; MA, myristic acid; DA, decanoic acid.

10.1021/bi048505f CCC: $27.50
Published on Web 09/25/2004

cycle of the parasite. This hypothesis is particularly relevant if one takes into account that there are only two available drugs against this disease (*8*).

The FABPs constitute a multigenic family of low molecular mass proteins (14−15 kDa). Analysis of 3D structures of FABPs revealed basic structural similarities among the members of this family despite low sequence identities (*9*). The actual physiological role of FABPs is still incompletely clear, and different hypotheses have been proposed, including protection of cell membranes and enzymes from the effect of high concentrations of free fatty acids (FAs) and of their acyl-CoA derivatives, storage of FAs, lipid trafficking, and regulation of cell growth and differentiation (*10*, *11*). Ambiguities mainly originate from the observation that these proteins can bind many different hydrophobic substrates (FAs, monoglycerols, diacylglycerol phosphates, lipooxygenase metabolites of arachidonic acid, acetyl Co-A, retinoids, and even heme (*12*)); also, FABPs are able to reversibly associate with artificial phospholipid bilayers, releasing or uptaking ther ligands (*11*). Thus, a very credible hypothesis on the functional role of FABPs suggests that these are involved in the intracellular trafficking of lipids to and from cell membranes; an important piece of evidence is that the heart fatty acid uptake is decreased in heart-fatty acid binding protein gene-ablated mice (*13*). The important metabolic role of FABPs and structural similarity of FABPs in evolutionary related parasites may explain why immunization with Sm14 confers significant levels of cross-protection against infections with *Schistosoma mansoni* and *Fasciola hepatica* in animal models (*6*).

Despite the importance of Sm14 as a vaccine and drug target candidate, there is still little structural and functional data about this protein. Thus, in this work, the 3D structures of the complexes of Sm14 with ACD and oleic acid (OLA) were solved by means of X-ray crystallography at 2.4 and 1.85 Å, respectively. Moreover, we characterized the binding and release reactions of Sm14 and several important FAs using 1,8-anilinonaphthalenesulfonic acid (ANS) as a competitor. The ligand with highest affinity, when water solubility is taken into account (*14*), is ACD, a compound essential to schistosomes. ACD is incorporated by the parasite more readily than other lipids (*15*) and is the immediate precursor of eicosanoid hormones, including the prostaglandins, critical in facilitating the skin penetration process of cercariae (*16*). Kinetic experiments were performed to clarify the mechanism of competition between FAs and ANS; a ternary complex between the protein and the two ligands was postulated to account for the complex reaction mechanism. Since affinities for FAs were shown to be pH dependent, pH jump experiments were performed which proved the presence of a slow pH dependent conformational change, whose physiological relevance is also discussed.

A comparison of the functional data and the two structures obtained by X-ray crystallography explains the structural basis of ligand selectivity. Indeed, ACD establishes a series of tight specific interactions, among which the most important one is a strong directional π-cation interaction between the guanidinium group of Arg 78 and the C8−C9 double bond. The shape and volume of the binding cavity is practically unchanged in the two complexes, but seems best adapted to bind ACD. Finally, the 3D structures of Sm14 also allowed us to structurally highlight two previously described antigenic determinants of the protein.

EXPERIMENTAL PROCEDURES

Cloning of Full-Length Sm14. *S. mansoni* adult worms were freshly obtained by perfusion of mice, infected at least 7 weeks before, using HEPES-buffered RPMI-1640 medium and containing 100 units/mL of heparin. Parasites, suspended in a minimal amount of medium, were frozen in liquid nitrogen and ground to a fine powder. Total RNA was extracted in Trizol reagent (Invitrogen) of which 5 μg was treated with SuperScript II reverse transcriptase (Invitrogen) to synthesize cDNA, following the protocol recommended by the manufacturer. To obtain the Sm14 full length coding region, a PCR reaction was carried out on the cDNA template using the forward primer 5′-GTTGAAACATATGTCT-AGTTTCTTGGGA-3′ and the reverse primer 5′-TTGCTC-GAGTTAGGATAGTCGTTTATAATT-3′. The PCR reaction was carried out using 1 μL of template, 50 pmol of each primer, and 2.5 units of Pfu DNA polymerase (Stratagene). The PCR product obtained was subcloned into pPCRscript Amp SK(+) (Stratagene), after which the plasmid was sequenced with an ABI PRISM 310 genetic analyzer using the BigDye Terminator Cycle Sequencing Kit (ABI). The same PCR product was then cloned into the Gateway His-tagged *Escherichia coli* expression vector, pDEST17 (Invitrogen), following the protocol recommended by the manufacturer. Expression of recombinant protein was carried out in *E. coli* BL21(DE3)pLysS cells.

Purification of Sm14. Wet cells of a 3 L bacterial growth were resuspended in 40 mL of buffer A (0.5 M NaCl, 50 mM Tris/HCl pH 8.0, 2 mM β-mercaptoethanol, 1 mM EDTA, 2% Triton X-100, and 1 mM protease inhibitor phenylmethylsulfonyl fluoride) (Sigma-Aldrich, all reagents were of analytical grade). Cell lysis was achieved after 5 min sonication at 4 °C. The protein was found to be expressed in inclusion bodies; hence, after centrifugation at $10000\times g$ and removal of the supernatant, the remaining pellets containing inclusion bodies were cyclically treated three times with the protocol described. Water washing of the residual pellet was employed to remove the excess detergent. The pellets were then dissolved in 50 mL of buffer B consisting of 6 M urea, 20 mM Tris/HCl pH 7.8, 500 mM NaCl, 5 mM imidazole, and 20 mM β-mercaptoethanol and gently stirred overnight at 4 °C. The resulting solution was filtered with a 0.45 μm syringe filter and loaded onto a Ni^{2+} column (chelating sepharose, Amersham Biosciences). The bound protein was washed with 5−7 column volumes of buffer B without β-mercaptoethanol. A rapid change of solution with buffer C (20 mM Na-phosphate pH 7.8, 500 mM NaCl) resulted in a properly folded His-tagged Sm14, which was eluted at about 250 mM imidazole by a linear gradient obtained by mixing buffer C with the same containing 500 mM imidazole. SDS−PAGE (*17*) showed the presence of the pure His-tagged Sm14 characterized by a molecular mass of 18.5 kDa. Then, 50 mg of pure His-tagged Sm14 was dialyzed against 100 mM Tris/HCl pH 8.0, 250 mM NaCl, at 4 °C, concentrated to 3.5−5 mg/mL followed by addition of 0.1% octyl-β-glucopyranoside. The protein solution was then diluted 1:1 with buffer D (2 M urea, 400 mM NaCl, 100 mM Tris/HCl pH 8.0, 10 mM $CaCl_2$, 2 mM β-mercaptoethanol), and 10 units/mL of

Table 1: Summary of Data Collection and Refinement

	Sm14−OLA	Sm14−ACD
space group	$P2_12_12$	$P2_12_12$
no. of unique reflns	13179	5746
$I/\sigma(I)$	22.3 (4.8)[a]	19.6 (8.8)[b]
completeness (%)	99.3 (92.7)[a]	95.5 (86.9)[b]
redundancy	4.5	5.5
unit cell dimens		
a (Å)	43.26	42.29
b (Å)	92.39	91.01
c (Å)	36.22	35.33
R_{merge}	0.046 (0.38)[a]	0.067(0.17)[b]
Ramachandran plot		
most preferred	116	110
allowed	7	13
generously allowed	0	0
disallowed	0	0
R	0.19	0.21
R_{free}	0.24	0.28
rms deviations		
bond lengths (Å)	0.02	0.015
bond angles (deg)	1.6	1.4
final model composition		
no. of protein atoms	1071	1057
no. of water molecules	209	76
no. of ligand molecule	1 (OLA)	1 (ACD)

[a] Last shell (1.88−1.85 Å). [b] Last shell (2.49−2.40 Å).

thrombin from bovine plasma (Sigma-Aldrich) was added. The resulting solution was stirred overnight at room temperature, then dialyzed against 0.1 M MES pH 5.5, and loaded onto a cation-exchange column (Source S-15, Amersham Biosciences). The cleaved Sm14 was eluted with a NaCl gradient at about 100 mM salt and verified by SDS−PAGE.

Crystallization of the Complex with FAs. Prior to crystallization the protein was equilibrated in 10 mM MES pH 5.5, 50 mM NaCl, 1 mM β-mercaptoethanol. The complexes with the two FAs were formed by adding a 2-fold molar excess of each ligand to Sm14. FAs were added in ethanol to a 1 mg/mL solution of Sm14, so that the ethanol concentration did not exceed 1% v/v. The mixture was gently stirred overnight at room temperature, after which the excess of ligands was removed by washing the sample in 3 kDa cutoff ultrafiltration devices (Amicon) and the protein was subsequently concentrated to 10 mg/mL. Crystallization was achieved using the hanging drop vapor diffusion method, employing drops consisting of 1 μL of a well solution of 0.1 M MES pH 6.0, 0.2 M Na acetate, 29−31% PEG 8K (w/v), 5 mM β-mercaptoethanol, and 1 μL of the protein sample. Rodlike crystals of dimensions 0.4 × 0.2 × 0.2 mm grew within a few days at 21 °C. Crystals were cryoprotected by using a solution containing 10% glycerol (v/v), 30% PEG 8K, 0.1 M MES, 0.2 M Na acetate, 5 mM β-mercaptoethanol, pH 6.0 and flash-frozen in liquid nitrogen.

Data Collection and Processing. Data for the two structures were collected at Elettra (Trieste, Italy) at 100 K and then processed using the HKL suite (*18*). Both Sm14−OLA and Sm14−ACD complexes crystallized in the same $P2_12_12$ space group with the unit cell dimensions given in Table 1. The datasets from 20.0 Å to 1.85 Å for Sm14−OLA and from 20.0 Å to 2.4 Å for Sm14−ACD are complete, well measured, and uniformly distributed in reciprocal space. Solvent volume was calculated, with the method of Matthews (*19*), to be around 45% of total crystal volume, and in both cases there was only one complex molecule per asymmetric unit.

Structure Solution and Refinement of Sm14−OLA Complex. The structure was solved by molecular replacement techniques with the program AMoRe (*20*) of the CCP4 suite (*21*), using the structure of the M-FABP complex (PDB code 2HMB; ref *22*) as search model after removal of FA and water molecules. Data between 15 Å and 3.5 Å were used and gave a clear solution with a correlation coefficient of 0.42. Model building and electron density map inspection were performed with the program XtalView (*23*). For model building both $2|F_o| - |F_c|$ and $|F_o| - |F_c|$ electron density maps were calculated and contoured at 1σ and 3σ levels, respectively. Most of the loops and the two α-helices were rebuilt. Subsequent rounds of rebuilding and refinement using Refmac (*24*), for 13179 reflections between 20.0 Å and 1.85 Å, resulted in a complete model of Sm14−OLA complex, with an *R* value of 0.198 and an R_{free} value of 0.246 (see Table 1). OLA, Met 20, and the side chains of His 14, Glu 110, Asp 124, and Lys 132 were refined with two alternative conformations. Two additional amino acids (Gly and Ser) resulting from the thrombin cleavage of the polyHis tag were found at the N-terminus.

Structure Solution and Refinement of Sm14−ACD Complex. Since this complex was isomorphic to Sm14−OLA, the difference Fourier method was used to solve the structure, using Sm14−OLA, without OLA and waters as a model. The refinement of Sm14−ACD proceeded in a fashion similar to that described above. The difference density located in the binding cavity was modeled as C20:4 fatty acid. Final refinement led to an *R* factor of 0.213 and an R_{free} value of 0.283 for 5746 reflections between 20.0 Å and 2.4 Å. The final structure contained 135 amino acid residues, 77 water molecules, and 1 molecule of ACD (see Table 1) and displayed only the side chains of Met 20 and His 14 in double conformations.

Structural Analysis. The models were monitored for geometrical quality by using PROCHECK (*25*). The *B* factors for several structural elements were calculated using the subroutine BAVERAGE of the CCP4 program (*21*). The contacts between FAs, residues, and waters were considered up to 4.6 Å and measured with the program CONTACT (*21*). The rms deviations between structures were calculated with the program LSQKAB (*21*). Volume and surface of the protein cavity were calculated with Cast-P (*26*). Sm14−OLA and Sm14−ACD structures have been deposited in the PDB with entry codes 1VYF and 1VYG, respectively.

Spectrofluorimetry and Fluorescence-Based FA Binding. The affinity of Sm14 for FAs was determined by taking advantage of the enhancement of the fluorescence quantum yield of ANS (Sigma-Aldrich) upon binding to Sm14 (*27*). The experiments were carried out using a Spex Fluoromax spectrofluorimeter at 20 °C in 2 mL of 0.1 M MES pH 5.5. Sample solutions of Sm14 were prepared by diluting a stock to concentrations of 0.1 μM for K_d determinations and to 5 μM for stoichiometric experiments. The stock solution (7 mM) of the fluorescent probe was prepared in ethanol. Aliquots of appropiately diluted solutions of ANS in 0.1 M MES were added to the protein and mixed in a cuvette with a magnetic stirrer for 2 min before spectra were collected. ANS and protein concentrations were verified spectrophotometrically (ϵ_{280} = 12750 M^{-1} cm^{-1} for Sm14, ϵ_{280} = 4990

Table 2: Equilibrium Constants for the Dissociation of Six Fatty Acids from Sm14 and Geometrical Parameters of Sm14−OLA and Sm14−ACD

fatty acid		CMC[a] (nM)	K_d (nM)	surfaces (Å^2) cavity	surfaces (Å^2) fatty acid	cavity vol (Å^3)
decanoic acid	(C10:0)		6100			
myristic acid	(C14:0)		88			
palmitic acid	(C16:0)	4000	33			
oleic acid	(C18:1)	6000	9	467.9	521.2	318.9
linoleic acid	(C18:2)	13000	24			
arachidonic acid	(C20:4)	20000	10	441.1	608.2	300.1

[a] Critical micellar concentration (*28*).

M^{-1} cm^{-1} for ANS in water). The excitation wavelength was 380 nm, and emission spectra were collected over the range of 400−500 nm; emission peaked at 480 nm, and readings between 470 and 490 nm were used for quantitative analyses. A 1:1 stoichiometry was achieved and the K_d determined to be 0.5 μM, without significant dilution of the Sm14, assuming simple equilibrium binding between aqueous ANS and Sm14.

Competition experiments with FA were performed as described for the ANS binding measurements, starting with a protein solution containing 4.5 μM ANS as competitor. OLA, ACD, palmitic (PA), myristic (MA), linoleic (LA), and decanoic acid (DA) were purchased from Sigma. All the FAs were dissolved in ethanol to a final concentration of 10 mM, then diluted in the experimental buffer prior to use, and used within a few hours. The concentrations of PA, LA, OLA, and ACD at the end of the titration were much below their CMC determined at physiological pH (*28*); presumably this applies also to DA and MA, whose CMCs have not been reported. Addition of FA aliquots resulted in quenching of the emission peak of the bound ANS. Titration curves were fitted to a simple replacement equation; the relative errors of the resulting K_d values (Table 2) lie within 0.2%.

Kinetic Measurements, pH Jump and Double Mixing Experiments. Stopped-flow experiments were carried out using an Applied Photophysics MV18 (Leatherhead, U.K.) apparatus equipped for fluorescence signal detection. The excitation wavelength was 380 nm, and emission was collected using a filter with cutoff ≤ 455 nm. Solutions of Sm14 (0.4 μM) in 0.1 M MES pH 5.5 were mixed with buffered solutions of ANS at concentrations ranging between 3 and 10 μM at 20 °C. The time courses were fitted to a double exponential.

The competition measurements were performed in two ways: Sm14 0.4 μM was first incubated with ANS 50 μM and mixed with different amounts of OLA (1.25−5 μM); alternatively the protein was incubated with OLA (1.5 μM) and mixed with different solutions of ANS (100 to 400 μM). These experiments were carried out under suboptimal conditions, given that the transmittance of the samples ranged from 56% to 10%. As a consequence the amplitude of the recorded signal cannot be trusted, whereas the rate constants are reliable.

In pH jump experiments, a weakly buffered Sm14 solution (0.4 μM) containing ANS at a concentration ranging from 2 to 3.3 μM at one pH (10 mM Mes pH 5.5 or 10 mM Hepes pH 7.4) is mixed with an equal volume of a concentrated buffer solution at the reciprocal pH (0.1 M Hepes pH 7.4 or 0.1 M Mes pH 5.5). The final pH of the solutions after the pH jump was assessed by mixing equal quantities of the buffers.

Double mixing experiments were carried out in order to test the time course of the pH dependent conformational change. Sm14 (0.4 μM) dissolved in 10 mM HEPES pH 7.4 was mixed with 0.1 M Mes pH 5.5, and the solution was "aged" for different times (ranging from 15 ms to 150 s). After the preset delay, the resulting solution was mixed with an equal volume of a buffer containing 0.1 M Mes pH 5.5 and 4 μM ANS.

RESULTS

Overall Structure of Sm14−FA Complexes. The complexes of Sm14 with ACD and OLA were crystallized under the experimental conditions described in the Experimental Procedures section. We also attempted to crystallize the FA-free Sm14 without success. The 3D structures of Sm14−ACD and Sm14−OLA were solved at 2.4 and 1.85 Å, respectively, by X-ray crystallography with the two models achieving final *R* factors of 21.3% and 19.8%, respectively. As assessed by the program PROCHECK (*25*), the stereochemical parameters of the two structures lie within the mean reference values (see Table 1 for a summary of crystallographic data). The protein main chain atoms and all the protein atoms of the two complexes of Sm14 are superimposable, with an rmsd of 0.32 Å and 0.75 Å, respectively. At the N-terminus both structures have two partially disordered amino acids, belonging to the linker region after the His tag (see Experimental Procedures). Numbering of the amino acids starts from the first native residue (Met 1), and the two non-native residues are called Gly −1 and Ser 0.

Similarly to the heart group of FABPs (H-FABPs), Sm14 folds as a twisted V-shaped β-barrel, formed by 10 antiparallel β-strands named from A to J (following the annotation of Sacchettini et al. (*29*)), closed on one side by interactions between the side chains and capped on the other side by a helix(I)−turn−helix(II) motif (Figure 1, panels A, C).

The two complexes have one single molecule of either ACD or OLA, bound in a large internal cavity. The volume of the cavity (calculated after removal of FA and waters from the models) is ∼300Å^3 (see Table 2), comparable to the cavity volumes of other FABPs belonging to the same family (*7*).

The gateway for entry of the substrate in the internal cavity is formed by the helix(I)−turn−helix(II) motif (residues 16−35) and by two hairpin loops between strands C−D and E−F (residues 56−58 and 74−78, respectively) (Figure 1). In both complexes, the gateway is closed and leaves no room for exit of the bound FAs; we hypothesize that diffusion of FAs into and out of the cavity requires opening of this doorway. In both structures Phe 57 on the C−D loop, previously proposed to be a key residue in the binding process (*30*), closes the entry of the lid, it is oriented toward the interior of the cavity, and its ring is at 3.5 Å to 4.5Å distance from the aliphatic chain of both OLA and ACD, respectively. In Sm14−OLA complex, Phe 57 has a higher *B* factor (41.1Å^2) as compared to the overall *B* factor of the protein (36.1 Å^2), index of certain mobility, whereas in Sm14−ACD, Phe 57 has a *B* factor (53.6Å^2) similar to that of the whole protein.

On the rim of the portal region, Lys 22 at the end of helix-(I) and Lys 58 on the C−D loop have the same relative

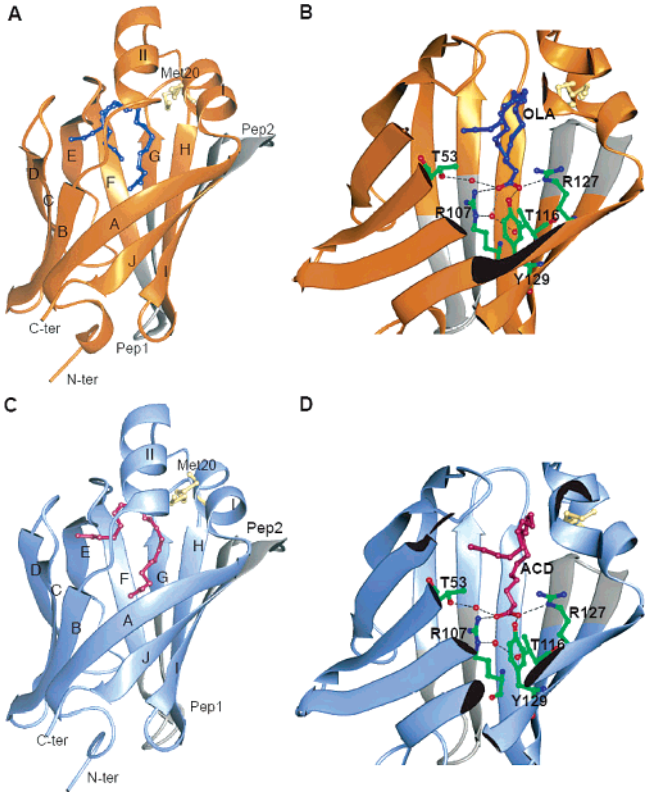

FIGURE 1: 3D structures of Sm14−OLA and Sm14−ACD complexes. (A) Overall structure of Sm14−OLA with secondary structure elements highlighted. Bound OLA (in blue ball-and-stick) is shown in its double conformation. Secondary structure elements and the corresponding residues: Gly 6-His 14 β-strand A, Phe 16-Leu 23 α-helix I, Ala 28-Thr 35 α-helix II, Thr 39-Asp 45 strand B, Lys 48-Ser 55 strand C, Lys 58-Cys 62 strand D, Phe 70-Lys 73 strand E, Asn 79-Lys 86 strand F, Lys 91-Asp 98 strand G, Asn 101-Asp 110 strand H, Thr 113-Val 120 strand I, Ile 126-Arg 131 strand J. Residues belonging to the antigenic peptides are colored in light gray, and Met 20 is shown in magnolia ball-and-stick. (B) Zoom of the binding cavity with the network of H-bonds fixing the carboxyl headgroup of OLA highlighted. (C) Overall structure of the Sm14−ACD complex. Strands and helices are labeled as in A. ACD is shown in purple ball-and-stick. (D) Same as panel B, for Sm14−ACD complex.

position and orientation as their homologues in H-FABP (Lys 22, Lys 59), where they were shown to interact electrostatically with phospholipid headgroups and supposed to drag the carboxylate of FA toward the internal cavity (*31*). On the back of the α-helix lid, the hydrophobic side chains of Trp 27 and Ile 32 are exposed to the solvent. This unusual orientation allows Trp 27 to insert among the phospholipid tails, thereby helping membrane binding, as shown by Kennedy et al. (*32*) for *Schistosoma japonicum* FABP. In both our structures Trp 27 and Ile 32 have the same relative orientation, consistent with the hypothesis that they interact with the cell membrane.

Structural Features Related to Antigenicity. Vaccination trials in Swiss mice showed that two peptides derived from Sm14 are capable of inducing a level of protection comparable to that induced by the full length protein (*6, 33*). The two peptides, namely Pep1 (from residue 85 to 94) and Pep2 (from residue 118 to 125), are topologically far from each other in Sm14 crystal structure (Figure 1). Pep1, seen at the bottom of the model in Figure 1, encompasses F and G β-strands including the loop between them; Pep2 is also located in a loop, more precisely a β-turn between strands I and J, close to αI-helix. Most of the side chains of these peptides are exposed to the solvent except Leu 92 and Gln 94 of Pep1 and Val 118, Val 120, and Ala 125 of Pep2, all of which point to the interior of the protein. Our structure reveals that both peptides are β-hairpins, i.e., they possess a stable secondary structure motif possibly retained even when the peptides are cleaved from the protein; and their sequence is sufficiently different from the homologous human isoforms to be recognized as "nonself" (at most 33% and 28% sequence identity, respectively).

The residue at position 20 of Sm14 is relevant to antigenicity. In our protein this residue is Met, but a natural allelic variant containing Thr has been described (Sm14-T20). Ramos and co-workers (*34*) studied the effect of mutations of Met 20 to Ala and Thr with respect to antigenicity, and observed a different protective response against *S. mansoni* cercariae in mice. Sm14-M20 displayed greater antigenicity than wild-type Sm14-T20 and artificial mutant Sm14-A20. Met 20 (Figure 1) is at the beginning of αI-helix, but it is far from the two antigenic epitopes; thus its effect can only be indirect. In both our structures, Met 20 presents a double conformation, with 50% occupancy; in one conformation the sulfur atom lies in proximity with the C9−C10 double bond in Sm14−OLA (3.8Å) and of the C11−C12 double bond in Sm14−ACD (3.7 Å), whereas in the other it is found between the two helices (hence out of the FA binding site). The latter conformer may play a critical role in stabilizing the closed conformation of the pocket lid when a FA is bound. It is possible, but it is not obvious from our structures, that the reason of the higher antigenicity of Sm14-M20 over Sm14-T20 lies in its greater thermodynamic stability (*35*).

Structure of Bound Fatty Acids. The greatest energy contribution for FAs binding to FABPs is expected to be due to the extraction of the hydrophobic molecule from the aqueous solvent; specific interactions between the bound FA and amino acid side chains may be responsible for ligand selectivity. These were examined looking at the level of the internal surface of the cavity by comparing the structures of the OLA and ACD complexes. The cavity is lined by polar and hydrophobic amino acids, whose side chains are mostly oriented toward the interior of the protein.

Bound OLA is completely surrounded by protein atoms and by structural waters (Figure 1, panel B). The carboxylate is at H-bond distance with Arg 127 N(ϵ), with Tyr 129 OH and with two structural water molecules, W12 and W78. Although the relative orientation of the carboxylate is well maintained in most of the FABPs, the geometry of H-bonds in the binding site is often different.

Bound OLA is found in two conformations, which differ in the orientation of the last five carbon atoms (Figure 2, panel A). Conformer 1 is found to be in the same U-shaped conformation previously observed for other FABPs (*30, 36*) and occupies the same portion of the cavity. Conformer 2 displays a chain bending similar to that found for ACD in the Sm14−ACD complex (see below), with the last part of the aliphatic chain out of the plane defined by the rest of the molecule. The difference maps clearly show electron density for both conformations of OLA from the C14 to C18 atom of the aliphatic chain. The two conformers are compatible with only slight differences in the positions of the first thirteen carbon atoms (Figure 2, panel A). The

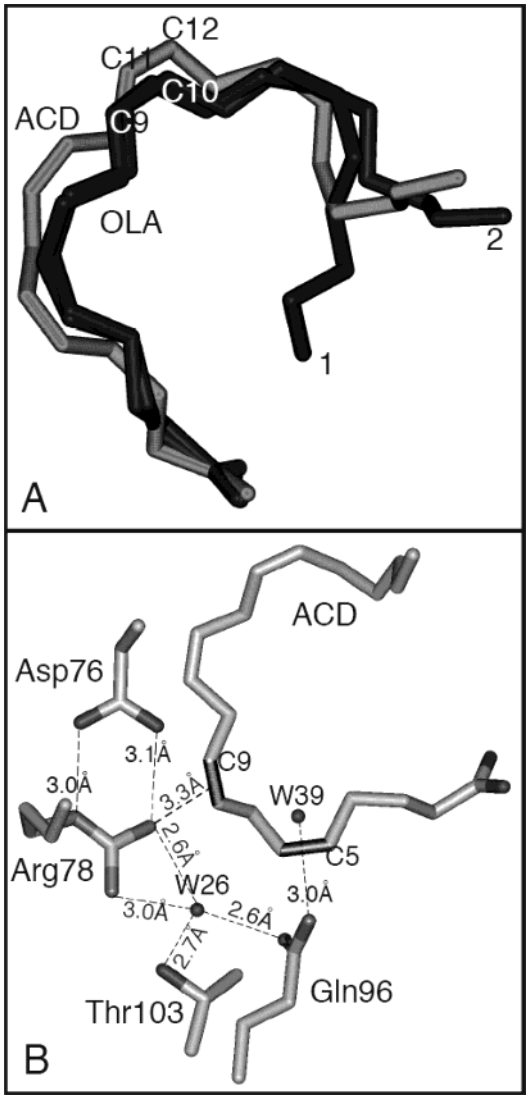

FIGURE 2: Structures of Sm14 bound OLA and ACD. (A) Representation of OLA and ACD bound to Sm14. The partial superimposition of the C9−C10 double bond of OLA (in dark gray) and the C11−C12 double bond of ACD (in light gray) demonstrates a similar configuration of the two FAs in the binding pocket. OLA displays a double conformation (shown as 1 and 2). In conformer 2 the aliphatic chain adopts a fold similar to the ACD in which the last carbon atoms of the tail are out of the plane defined by the rest of the molecule; in conformer 1 the last carbon atom of OLA points toward the carboxylic moiety, yielding a V-shaped conformation. (B) Network of contacts in the binding site of the Sm14−ACD complex. The indicated residues interact with the double bonds of ACD in C5 and C8. The same overall architecture is conserved in the Sm14−OLA complex.

relative occupancy of the two conformers is 50%, and their average *B* factors (43 Å^2) are above the average *B* factor of the side chains of the surrounding cavity (33 Å^2). Moreover, in conformer 1, OLA is disordered at its terminus, as indicated by the interruption of the electron density map between C15 and C16.

The hairpin conformation of bound OLA is induced by the cis double bond between C9 and C10, and by gauche bonds between C5 and C6, C13 and C14, and stabilized by a large number of van der Waals interactions with the protein side chains and with 7 ordered water molecules in conformer 1 and 6 in conformer 2. In both conformers the C9−C10 double bond interacts with the conserved Phe 16 and Met 20 (only in one of the two conformations of Met20) and with Val 25, Ser 75, Asp 76, Arg 78.

Of the 21 residues that contact OLA in conformer 1, 10 are hydrophobic and 11 are polar. In detail: 8 residues belong to 4 of the 10 β-strands (Gln 96 on G β-strand; Thr 103, Ile 105, Arg 107 on H; Thr 116, Val 118 on I; and Arg 127, Tyr 129 on J), 3 of these amino acids (Arg 107, Arg 127, and Tyr 129) constitute the binding site of FA carboxylate, 2 residues (Val 36, Pro 38) come from the loop that connects helix(II) with B β-sheet, 4 lie on the mobile loops that form the rim of the β-barrel (Phe 57 in C−D loop; Ser 75, Asp 76, and Arg 78 in E−F loop), and the remaining 7 belong to the helix(I)−turn−helix(II) motif (Phe 16, Met 20, Leu 23, Val 25, Thr 29, Ile 32, Gly 33).

ACD, like OLA, is entirely buried within the cavity, but it has a single conformer with a 100% occupancy. The electron density map is complete without interruption. Interestingly ACD is characterized by an average *B* factor (37 Å^2) lower than that of the surrounding polypeptide chain (48 Å^2). The carboxylic moiety makes the same types of contacts as OLA (Figure 1, panel D) and assumes a conformation similar to OLA conformer 2, making the same contacts, plus some additional ones. The contacts between ACD and the side chains of Thr 53, Ser 55, Lys 58, and Leu 60, characteristic of OLA conformer 2, are maintained although closer in space. Moreover, the long chain of ACD and the presence of four cis double bonds make its structure rigid, force its convex shape, and consequently increase the contact surface between the protein and the lipid, as compared to OLA (Figure 2, panel A). Several specific sets of contacts with side chains and water molecules stabilize the four double bonds (i.e., Phe 16, Met 20, Leu 23, Val 25, Thr 29, Gly 33, Phe 57, Ser 75, Asp 76, Arg 78, Gln 96, Thr 103, Ile 105, W26, W39).

In both ACD and OLA complexes, residue Met 20 adopt two alternative side chain conformations; in one of those Met 20 is closer to the double bond of the bound FA (C9−C10 for OLA and C11−C12 for ACD). The double bonds at C9−C10 in OLA and at C11−C12 in ACD are found in the same position (Figure 2, panel A), interacting with the same amino acids but in closer contact in the ACD adduct. This is indicative of how different FAs arrange their aliphatic chain for a better fit into the same protein pocket.

Relative to the overall plan defined by the lipid, the first two double bonds (C5−C6, C8−C9) of ACD are out of the plane, whereas the last two lie in it. Examination of the protein−ligand interactions shows that specific polar contacts stabilize the first two cis double bonds in that out-of-plane orientation (Figure 2, panel B; Figure 3, panels A, C). It is interesting to note the continuous contact surface generated by the side chains and by the two waters interacting with the first two double bonds of ACD. This architecture is maintained in Sm14−OLA structure, but it is not suitable to allow specific interactions with a C18:1 FA.

The mobility of the E−F loop is a relevant structural element of FABPs since it controls the access of the FA to the internal cavity (*37*). In Sm14 and the FABPs belonging to the H family, the role of the E−F loop is even more important since it bears the residues Thr 74, Asp 76, and Arg 78. Our structures demonstrate that Arg 78 establishes a strong, directional π-cation interaction with C8−C9 double bond of ACD (Figure 2, panel B; Figure 3, panel A), whereas

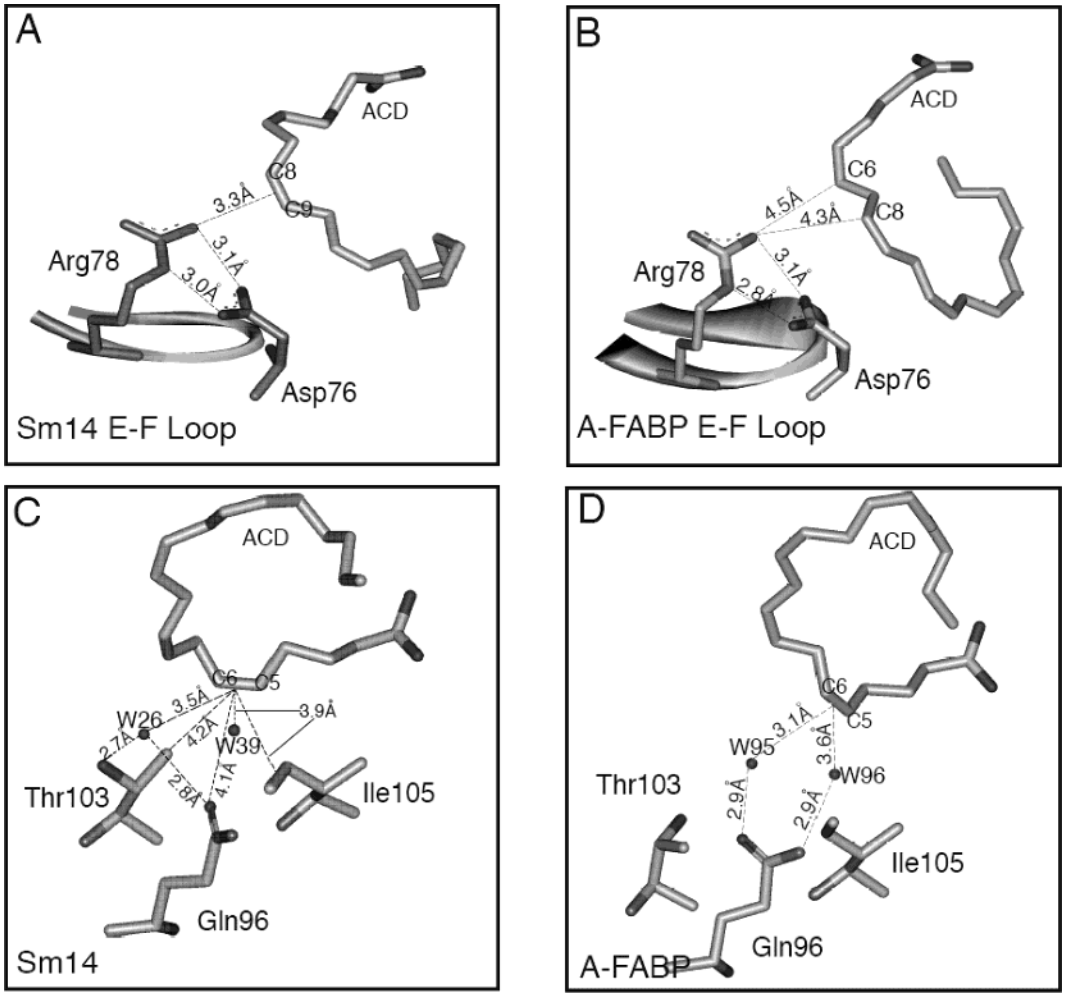

FIGURE 3: Detail of the interactions between Sm14 and ACD. (A) Network of interactions between Sm14 and ACD C8−C9 double bond. Residues belonging to the E−F loop are highlighted. H-bonds between Asp 76 and Arg 78 keep the terminal NH2 of Arg 78 in orbital overlap with C8−C9 double bond. (B) Network of interactions between residues belonging to the E−F loop of murine A-FABP (1ADL, LaLonde et al., 1994) and bound ACD, in the same orientation as in panel A. ACD is bound with a different geometry; hence the conserved Arg 78 loosely contacts the region between C5−C6 and C8−C9 double bonds. (C) The Sm14−ACD complex has been rotated by 180° around the *x* axis with respect to panel A to show the contacts between the pocket and C5−C6 double bond. Interaction distances have been measured between conserved residues and water molecules and the π orbital of the double bond. (D) Same as in C for the A-FABP−ACD complex. In this case only one of the conserved residues contacts ACD via the two water molecules.

Thr 74 and Asp76 are involved in a network of H-bonds that helps in bending the E−F loop toward the interior of the protein and hence toward ACD. Moreover, Asp 76 establishes a double H-bond with Arg 78 that stabilizes the position of the latter in close proximity with the bound FA (Figure 3, panel C). Consistently, in the complex with OLA, which lacks the double bond at C8−C9, the interaction between FA and Arg 78 is looser with the *B* factors of E−F loop greater by about 10 Å^2 with respect to the mean value of the whole protein, whereas in the Sm14−ACD structure they are in the same range as the overall structure.

In conclusion, the binding pocket is relatively rigid and does not change upon binding different ligands; OLA and ACD are accommodated in the pocket with respectively lower or higher shape complementarity, due to their intrinsic geometrical and stereochemical parameters.

Ligand Binding Properties of Sm14. Previous work by Moser et al. (*4*) showed that Sm14 binds ^{14}C-labeled palmitic and linoleic acid at physiological pH, with dissociation equilibrium constants of ~2 μM. Using the environment-sensitive fluorescent probe ANS, we carried out a thorough equilibrium and kinetic investigation of complex formation between Sm14 and six FAs, differing in length and degree of saturation,. Binding of ANS to Sm14 is associated with a substantial increase in fluorescence intensity and a blue shift of the maximum emission, indicative of transfer from water to an apolar environment (*38*). Moreover, the crystallographic structure of the adduct of ANS with murine adipocyte lipid binding protein (A-FABP) shows that this probe is located in the FA's binding site with the sulfonate moiety placed between the two arginines involved in the FA's carboxylate binding site (see ref *39* and above). Given the low solubility of FAs and the high affinity of FABPs for these ligands, a method based on a competitive fluorescent probe seemed ideally suited to determine formation of a complex between Sm14 and various ligands.

The functional properties of Sm14 were initially characterized at pH 7.4 and 5.5. The acidic pH was preferred for three reasons: (i) the equilibrium isotherm of the reaction between ANS and Sm14 at physiological pH (7.4) is complex and suggests a stoichiometry greater than 1; on the other hand, at pH 5.5, Sm14 binds ANS with 1:1 stoichiometry and high affinity (K_d = 0.5 μM); (ii) at this pH the protein is stable for a long time; and (iii) crystals of Sm14 were obtained at

a similar pH (see Experimental Procedures), hence granting a better comparison between functional and structural data. For comparison, the K_d values reported for ANS binding to A-FABP and I-FABP ranged from 1 to 50 μM, under different conditions (*27*, *38*).

Addition of FAs to the Sm14−ANS complex quenches emission at 475 nm, indicating that FAs displace ANS. The best fit analysis of the titration data is compatible with a single FA molecule binding. The values of K_d calculated for 6 FAs are reported in Table 2. The results show that formation of the complex between Sm14 and OLA or ACD has essentially the same dissociation constant: 9 and 10 nM, respectively. The K_d values for decanoic, myristic, palmitic, and linoleic acids are respectively 610-, 9-, 3-, and 2.5-fold greater than for OLA and ACD. The maximum ANS quenching found in our experiments occurs at concentrations much below the FA critical micellar concentrations (CMC) as determined at pH 7.4 under physiological conditions (*28*). This is important since above the CMC the equilibrium becomes heterogeneous.

The high affinity of FABPs for their ligands is explained because (i) FAs are poorly soluble in water; hence there is a favorable free energy change associated with their transfer to the less polar protein interior; (ii) FAs establish extensive, though weak, contacts with the residues lining the internal cavity of FABPs, accounting for enthalpic contributions to binding; (iii) given their low pK_a ($\approx$4.7), FAs are predominantly in the anionic form, both at pH 5.5 and at pH 7.4, thus favoring the interactions with the conserved positively charged guanidinium group of Arg 127 (see the section on the structure above). However, these same considerations challenge the data reported in Table 2, because one would expect that the lower the solubility of a given FA, the higher the apparent affinity. Indeed, this occurs in several FABPs that bind FAs with affinities correlated to their solubilities (*14*), i.e., in agreement with the expectation that the greater energy contribution to binding comes from the extraction of the poorly soluble FA from the aqueous phase. The case of Sm14 and unsaturated FAs violates this rule, and ACD is particularly noteworthy since its critical micellar concentration is relatively high, yet its K_d is the lowest in the group (together with that of OLA). This result is explained by the structure of the Sm14−ACD complex, which reveals specific interactions at the level of the two double bonds C5−C6 and C8−C9, thus implying a specificity for this physiologically important ligand.

ANS could not be replaced by prostaglandins, up to μM concentrations, proving that Sm14 does not bind these derivatives of ACD, even at concentrations higher than those prevailing under physiological conditions in the human body.

The differences between the K_ds reported in Table 2 at pH 5.5 and older data (*4*) can be rationalized by the difference in pH. Indeed, when the same ligand titration experiments were carried out at pH 7.4, we observed an increase in K_d by a factor of 10 or more. This reduction in affinity as pH increases is observed for both ANS and FAs and may be of physiological relevance in the release of bound FAs (see below).

Kinetics of Complex Formation. The kinetic rate constants for binding and release of ANS and OLA were determined by fluorescence stopped flow. When dealing with a carrier protein displaying such a high affinity for its ligands, the question arises whether release occurs to an extent and at a rate compatible with physiological requirements. At pH 5.5, ANS combination with Sm14 is fast, and its second-order rate constant is $\geq 2 \times 10^8$ M^{-1} s^{-1}, thus approaching the diffusion limit. Given the affinity of ANS ($K_d = 0.5$ μM) and the sensitivity of the instrument, it is impossible to dilute the ligand enough to obtain a more precise estimate. The kinetics of dissociation of ANS bound to Sm14 can be followed by displacement, adding an excess of OLA. The recorded time courses have half-times of $\sim$1 s and are best described by two exponentials, irrespective of the concentration of OLA (data not shown). Although it is obvious that the observed slow fluorescence decrease is associated with the release of ANS, it is unclear if the reaction involves a ternary complex with both ANS and OLA transiently bound to the protein cavity. Furthermore, the ratio between the overall k_{on} and k_{off} does not equal the equilibrium constant, suggesting a complex reaction mechanism.

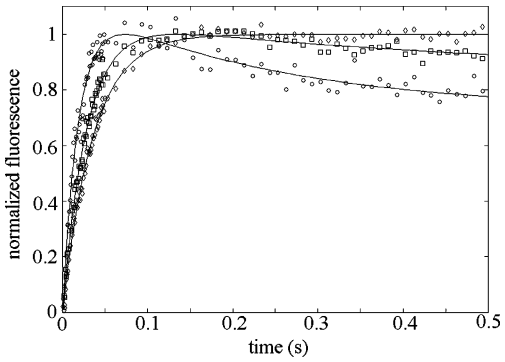

FIGURE 4: Time course of oleic acid replacement by ANS. Sm14 (0.4 μM) incubated with OLA (1.5 μM) in Mes pH 5.5 is rapidly mixed with ANS buffered solutions at concentrations of 100 (◇), 200 (□), and 400 μM (○). Experimental points are fitted with a model including a ternary complex between Sm14−OLA−ANS. The slow decrease in fluorescence signal (always present but best seen at the highest ANS concentration) is the dissociation of OLA from the ternary intermediate.

Release of bound OLA was achieved by rapidly mixing the complex with a 70- to 1000-fold excess of ANS (Figure 4). Even at the lowest concentration, ANS is able to displace over 50% of the bound OLA. The observed rate constants for the first process vary from 92 s^{-1} (at the highest ANS: OLA ratio) to 28 s^{-1} (at the lowest ratio), leading to an extrapolated dissociation rate constant for the complex between Sm14 and OLA of 200 s^{-1}. This value seems unreasonable because, given the high affinity of the complex ($K_d = 9$ nM), the calculated combination rate constant would have to be as high as 2×10^{10} M^{-1} s^{-1}. Therefore, we assume that the reaction mechanism is complex and involves a ternary complex of Sm14 with both ANS and OLA to the protein as an unstable intermediate, from which OLA would then dissociate. Accordingly, the main fluorescence increase (Figure 4) could be assigned to the second-order combination between the complex Sm14−OLA and ANS (rate constant of 3×10^6 M^{-1} s^{-1}), whereas the subsequent fluorescence decrease (rate constant of 3 s^{-1}) would be assigned to the dissociation of OLA from the ternary complex and the coupled entrance of water in the pocket. This hypothesis is consistent with data for *Echinococcus granulosus* FABP (EgFABP), a carrier with high sequence identity with Sm14, which at pH 7.4 binds more than one ligand (*40*). The rate

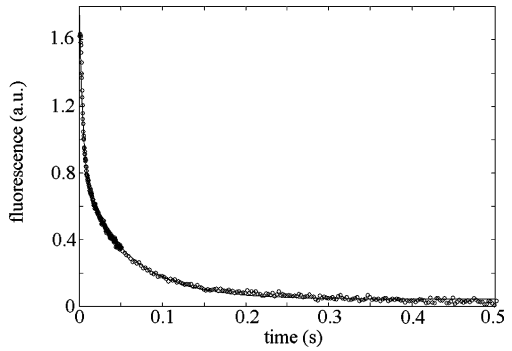

FIGURE 5: Time course of ANS release after a pH jump from 5.5 to 7.4: dissociation of ANS, following the pH jump 5.5→7.4, monitored by a decrease in fluorescence. A solution of 0.4 μM Sm14 containing 2 μM ANS in 0.01 M Mes buffer pH 5.5 was mixed in the stopped flow apparatus with an equal volume of 0.1 M Hepes buffer pH 7.4.

of release of the bound FA from Sm14 is independent of the ionic strength of the medium.

Since the affinity of Sm14 for its ligands depends on pH and decreases by over an order of magnitude as the pH is raised from 5.5 to 7.4, it is possible to induce ANS binding or release by rapidly changing the pH of the solution. Indeed if the Sm14−ANS complex in diluted buffer at pH 7.4 is rapidly mixed with concentrated buffer at pH 5.5, binding occurs; if the opposite pH jump is realized, the dissociation of ANS can be followed (Figure 5). It is often observed that pH changes affect the ligand affinity of proteins that function as carriers of small ligands; e.g., this occurs for hemoglobin and transferrin. Since this mechanism helps the protein to upload its ligand even when its concentration is low, and to download it even when its concentration is relatively high, therefore it seemed worth of detailed investigation.

Unexpectedly, after a pH jump the change in ligand affinity occurred at a relatively slow rate. Indeed, when Sm14 equilibrated in diluted Hepes buffer at pH 7.4 was rapidly mixed with a concentrated buffer at pH 5.5 containing ANS (Figure 6, panel A, trace 1), the binding time course was slower than that observed with Sm14 equilibrated at pH 5.5 and mixed with ANS at the same pH (Figure 6, panel A, trace 2). This shows that the low-pH conformation, corresponding to the fast reacting state, was not yet populated immediatly after the acidification to pH 5.5. To determine the rate constant of the pH dependent conformational change we carried out a double mixing experiment, in which Sm14 equilibrated in diluted buffer at pH 7.4 was mixed with concentrated buffer at pH 5.5 and then, after a variable delay, with ANS dissolved in buffer at pH 5.5. All time courses could be described by two exponentials whose rate constants are independent of the final pH while the relative amplitude of the two processes (corresponding to the two kinetic phases) was the only parameter that varied with pH. The results of this analysis are shown in Figure 6, panel B; the rate constant of the conformational change is 0.1 s^{-1}, i.e., possibly compatible with physiological requirements.

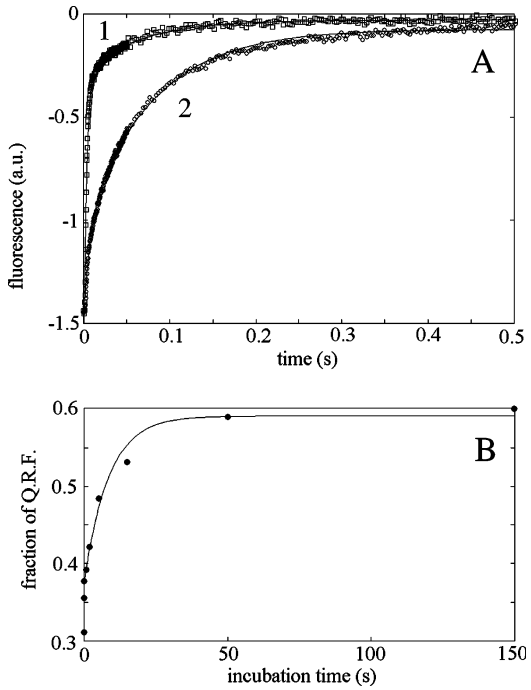

FIGURE 6: Time course of ANS combination after a pH jump from 7.4 to 5.5. (A) Trace 1: Binding of ANS at pH 5.5, monitored by an increase in fluorescence, is fast. A solution of 0.4 μM Sm14 in 0.1 M Mes buffer pH 5.5 was mixed with an equal volume of a solution of 3.3 μM ANS in the same identical buffer. Trace 2: The binding of ANS at pH 5.5 after an instantaneous pH jump 7.4→5.5 is quite different from trace 1, because the protein is still in the slowly reacting pH 7.4 conformational state; this was obtained by mixing a solution of 0.4 μM Sm14 in 0.01 M Hepes buffer pH 7.4 with an equal volume of a solution of 3.3 μM ANS in 0.1 M Mes buffer pH 5.5. Other conditions: $T = 20$ °C; excitation wavelength 380 nm, emission wavelength ≥ 455 nm. (B) Fraction of the quickly reacting form (QRF) of Sm14 as a function of the incubation time at pH 5.5 after a pH jump 7.4→5.5. A solution of 0.4 μM Sm14 in 0.01 M Hepes buffer pH 7.4 was first mixed with an equal volume of 0.1 M Mes buffer pH 5.5, and then, after variable incubation time, with a double volume of a solution of 4 μM ANS in 0.1 M Mes buffer pH 5.5. The time courses of fluorescence increase (indicating complex formation) were fitted to double exponentials under the assumption that the two kinetic rate constants were independent of the incubation time, while the relative amplitude of the fast and slow binding events changed. Each experimental point represents the fraction of fluorescence increase assigned to the faster kinetic process. The solid curve drawn through the experimental points is the best fit for a simple exponential relaxation to the equilibrium condition, with $\tau^{-1} = 0.1$ s^{-1}.

DISCUSSION

Sm14 is the only vaccine candidate shown to achieve significant immune protection against schistosomiasis as well as against the helminth infection of cattle caused by *F. hepatica* (*6*). The protein is present in all the stages of the life cycle of the parasite which occur in the definitive host, i.e., schistosomulum, adult worm, and eggs (*5*). In the adult worm the basal lamella of the tegument and the gut epithelium are strongly labeled by immunofluorescent probes against Sm14. These tissues have a high flow of lipids, supporting the putative role of Sm14 as an intracellular carrier of FAs (*4*). Therefore a detailed investigation of its structure and function is demanded and is reported in this paper.

Comparison with Other FABPs. FABPs are grouped according to sequence comparison. Within this classification, Sm14 belongs to the family group represented by H-FABP (mammalian heart, muscle, brain, adipose tissue, and myelin FABPs; parasite Sj- and Eg-FABP (*41*)). It seems that all these proteins have higher affinity for polyunsaturated FAs compared to those belonging to the I-FABP group, whose affinity correlates with the water solubility of different FAs

and, hence, decreases as the level of unsaturation increases (*14*).

The equilibrium dissociation constant of H-, B-, M-FABP is in the range 4−7 nM for OLA and 18−27 nM for ACD (14). In general our estimates fall within this range, although the affinity of Sm14 for ACD (K_d = 10 nM) remains the highest of the group. Interestingly, Eg-FABP (expressed by another parasite lacking de novo synthesis of FAs) shows a similar trend in affinities versus OLA, LA, and ACD (*40*). An important difference between Sm14 and the FABPs belonging to the heart group is that the affinity for FAs is maximal at acidic pH, whereas in the group of FABPs from mammals it is greater at physiological pH.

Several structures of FABPs are deposited in the PDB, most of them bound to FAs. The finding that FABPs (including Sm14) can be crystallized almost only in the liganded state implies that binding of FAs stabilizes the protein. This is now understandable by looking at the structures of Sm14 complexes with OLA and ACD (Figure 1), given that the flap constituted by the two helices is less mobile in the complex and seems to contribute to stabilize a more compact state. Only two structures of FABP complexes with polyunsaturated FAs are deposited in the PDB: human B-FABP (*36*) with docosahexanoic acid (DHA, 22:6) and murine A-FABP with ACD (PDB code: 1ADL (*42*)). The dissociation equilibrium constant measured for ACD binding to the latter protein is reported to be 4.4 μM (by means of calorimetry(*42*)) and 0.2 μM (by the acrylodated intestinal fatty acid binding protein ADIFAB method (*14*)). A comparison of the 3D structures of the complexes of Sm14−ACD and murine A-FABP−ACD (Figure 3, panels B, D) shows that the former is characterized by more specific and stronger contacts with the ligand than the latter, since, in spite of the fact that the relevant amino acid residues are conserved, their orientation is not. This shows the crucial role of the precise stereochemistry of residues in the binding site in determining the free energy of complex formation of ACD, as detailed below.

Binding Specificity of FAs to Sm14. The overall structure of Sm14 is a V-shaped β barrel (Figure 1) closed on the top by a lid of helices and on the bottom by side chains, similarly to other FABPs. The homology model of Sm14 without bound FA, presented by Tendler et al. (*6*), is in overall satisfactory agreement with our structures. Our results extend information on the structure and provide the details necessary to account for ligand affinity and specificity. Our data on the affinity of Sm14 for several FAs suggest that the protein is selectively designed to accommodate unsaturated FAs and, in particular, ACD. ACD is not synthesized by schistosomes (as the worm is incapable of FA biosynthesis), but its derivatives play an essential role in the evasion of the immunological defenses of the host (*16*); therefore, the preference of Sm14 for ACD may confer an evolutionary advantage to the parasite, and inactivation of Sm14 may have therapeutic consequences.

ACD is a priori a relatively difficult ligand for a FABP, since it is more soluble and less concentrated in the host's blood than other important FAs. The rigid structure of ACD demands a precise complementarity with the binding site of Sm14, and implies a minor change in entropy upon binding; on the contrary, OLA and saturated FAs are relatively mobile and binding to the protein cavity diminishes the entropy of their hydrocarbon tail. Comparison between the ACD and OLA complexes is instructive, since OLA retains some mobility inside the pocket and binding is favored by its lower solubility (Table 2); consistently, the average *B* factor of ACD is lower than that of the protein, whereas that of OLA is higher.

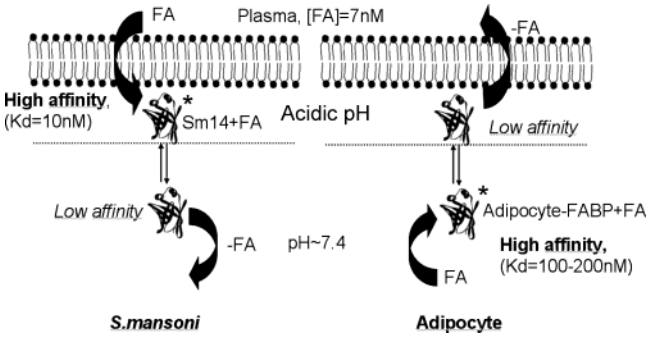

FIGURE 7: A schematic representation of the physiological implications of the pH−affinity dependence of FABPs in *S. mansoni* and in mammalian adipocytes. The scheme depicts the hypothetical principal direction of FA transport in *S. mansoni* tegument (left) and in mammalian adipocyte (right). The main functional difference between Sm14 and A-FABP (apart from their ligand specificity) is the opposite effect of pH (see text) that is suggested to determine the preferential direction of the FA trafficking in the two cases.

The crystallographic structure demonstrates a remarkable complementarity between ACD and the binding cavity of Sm14, involving (among others) a strong and highly specific π-cation interaction between the double bond at C8−C9 and the guanidinium group of Arg 78, in turn kept in a favorable stereochemistry by Asp 76. In addition, a specific network of interactions is established between the C5−C6 double bond of ACD and Gln 96, Thr 103, Ile 105, W26, and W39. Finally, the double bonds C5−C6, C8−C9, C11−C12, and C13−C14 are organized around Phe 18 in a optimal manner for π-stacking interactions. Other interactions, including those with the carboxylate head of the FA, are less specific and, although they may contribute to the overall free energy of binding, probably have a minor role in selecting among different FAs.

Structure−Function Relationship and Physiological Role. In view of the high affinity of Sm14 for OLA and ACD, we have addressed the physiologically significant question of the mechanism of release of these FAs. Our experiments demonstrate that the affinity of Sm14 for FAs is higher at acidic pH than at neutral or basic pH, which is opposite to the behavior observed in mammalian FABPs; e.g., A-FABP displays a higher affinity at alkaline pH (*43*), although its isoelectric point is similar to that of Sm14, suggesting a similarity in electrostatic interactions with membranes. Local pH changes inside the cell occur in proximity with the membrane due to the buffering power of the anionic phospolipid headgroups; the microenvironment near the membrane is thus more acidic than the bulk of the cytoplasm (*44*). Since the affinity of Sm14 is higher at lower pH, its main physiological role may be transfer or facilitated diffusion of ACD (and other FAs) from the external tegument membrane (i.e., from the contact interface with the host's blood) to the internal one (i.e., to the worm's body); on the other hand mammalian A-FABP in the adipocytes (whose interior is very rich in FAs) would transport FAs in the opposite direction. This is schematically shown in Figure 7,

where we have highlighted a possible scheme of FA transport in these two cases.

Over and above the pH dependent change in ligand affinity, we have documented that the kinetics are compatible with physiology and that the decrease in affinity at alkaline pH is coupled to a slow ($k \sim 0.1\ s^{-1}$) conformational change of the protein. This unexpected effect may be due to a widening of the protein cavity at pH 7.4, causing a reduction of affinity, an observation crucial to understand the role of Sm14. The free FA concentration in human blood is about 7 nM (*45*), compatible with the high affinity of Sm14 for ACD at the acidic pH prevailing in proximity with the cell membrane, whereas in the cytoplasm the release of ACD would be facilitated by the relatively higher pH. If we consider that the schistosome needs to uptake FAs from plasma whereas adipocytes need to discharge them, not only different affinities among different FABP families but also different pH dependences of affinity appear to us relevant to physiology. The reversible association of FABPs with the internal surface of the cell membrane further strengthens our hypothesis and suggests that their isoelectric point is physiologically important. H-FABPs are acidic proteins, L-FABPs are neutral, and M-FABP and murine A-FABP are basic (*10*). Sm14 is, however, unique because, although belonging to the H-FABP family (which is generally acidic), it has a p*I* = 7.8, which is similar to that of M-FABP and A-FABP, promoting the interaction with anionic membranes. Moreover, it has been shown that the uptake of FAs can also occur in close proximity with specific receptors (*11*) and it was recently reported that schistosomes express receptors for human lipoproteins that display acidic properties (*46*). These data support the hypothesis that Sm14 binds FAs from the host's blood and diffuses inside the tegumental cells to enhance their intracellular transport, exploiting the pH gradient between the microenvironment near the membrane and the bulk cytosol, as schematically summarized in Figure 7.

In conclusion, our findings demonstrate how much the lipid affinity, specificity, and pH dependence of FABPs may vary according to subtle differences in the amino acid sequence and especially the details of the 3D structure to suit the needs of the tissue or organism in which they are expressed. Within this range of characteristics, Sm14 is particularly suited to effect the uptake of FAs by the parasite from the host.

ACKNOWLEDGMENT

We thank Dr. Andrea Ilari for several helpful suggestions. We are grateful to Elettra (Trieste, Italy) for data collections and financial support.

REFERENCES

1. Brouwers, J. F., Smeenk, I. M., van Golde, L. M., and Tielens, A. G. (1997) The incorporation, modification and turnover of fatty acids in adult *Schistosoma mansoni*, *Mol. Biochem. Parasitol. 88*, 175−185.
2. Furlong S. T., and Caulfield J. P. (1989) *Schistosoma mansoni*: synthesis and release of phospholipids, lysophospholipids, and neutral lipids by schistosomula, *Exp. Parasitol. 69*, 65−67.
3. McKerrow, J., and Salter, J. (2002) Invasion of skin by schistosoma cercariae, *Trends Parasitol. 18*, 193−195.
4. Moser, D., Tendler, M., Griffiths, G., and Klinkert, M.-Q. (1991) A 14-kDa *Schistosoma mansoni* polypeptide is homologous to a gene family of fatty acid binding proteins, *J. Biol. Chem. 266*, 8447−8454.
5. Brito, C. F., Oliveira, G. C., Oliveira. S. C., Street, M., Riengrojpitak, S., Wilson, R. A., Simpson, A. J., and Correa-Oliveira, R. (2002) Sm14 gene expression in different stages of the Schistosoma mansoni life cycle and immunolocalization of the Sm14 protein within the adult worm, *Braz. J. Med. Biol. Res. 35*, 377−81.
6. Tendler, M., Brito, C. A., Vilar, M. M., Serra-Freire, N., Diogo, C. M., Almeida, M. S., Delbem, A. C., Da Silva, J. F., Savino, W., Garratt, R. C., Katz, N., and Simpson, A. S. (1996) A Schistosoma mansoni fatty acid-binding protein, Sm14, is the potential basis of a dual-purpose anti-helminth vaccine, *Proc. Natl. Acad. Sci. U.S.A. 93*, 269−73.
7. Bergquist, N. R., and Colley, D. G. (1998) Schistosomiasis Vaccines: Research to development, *Parasitol. Today 14*, 99−104.
8. Ferrari, M. L. A., Coelho, P. M. Z., Antunes, C. M. F., Tavares, C. A. P., and da Cunha, A. S. (2003) Efficacy of oxamniquine and praziquantel in the treatment of *Schistosoma mansoni* infection: a controlled trial, *Bull. W.H.O. 83*, 190−196.
9. Storch, J., and Thumser, A. E. (2000) The fatty acid transport function of fatty acid binding proteins, *Biochim. Biophys. Acta 1486*, 28−44.
10. Veerkamp, J. H, Peeters, R. A., and Maatman, R. G. (1991) Structural and functional features of different types of cytoplasmatic fatty acid-binding proteins, *Biochim. Biophys. Acta 1081*, 1−24.
11. Weisiger, R. A. (2002) Cytosolic fatty acid binding proteins catalyze two distinct steps in intracellular transport of their ligands, *Mol. Cell. Biochem. 239*, 35−42.
12. Kaikaus, R. M., Bass, N. M., and Okner R. K. (1990) Functions of fatty acid binding protein, *Experientia 46*, 617−630
13. Murphy, E. J., Barcelo-Coblijn, G., Binas, B., and Glatz, J. F. (2004) Heart fatty acid uptake is decreased in heart-fatty acid binding protein gene-ablated mice, *J. Biol. Chem. 279*, 34481−34488.
14. Richieri, G. V., Ogata, R. T., Zimmerman, A. W., Veerkamp, J. H., and Kleinfeld, A. M. (2000) Fatty acid binding proteins from different tissues show distinct pattern of fatty acid interactions, *Biochemistry 39*, 7197−7204.
15. Rumjanek, F. D., and Simpson, A. J. (1980) The incorporation and utilization of radiolabelled lipids by adult *Schistosoma mansoni*, *Mol. Biochem. Parasitol. 1*, 31−44.
16. Angeli, V., Faveeuw, C., Roye, O., Fontaine, J., Teissier, E., Capron, A., Wolowczuk, I., Capron, M., and Trottein, F. (2001) Role of the parasite prostaglandin D_2 in the inhibition of epidermal Langherans cell migration during schistosomiasis infection, *J. Exp. Med. 193*, 1135−1147.
17. Laemmli, U. K. (1970) Cleavage of structural proteins during the assembly of the head of bacteriophage T4, *Nature 227*, 680−685.
18. Otwinowsky, S., and Minor, W. (1996) Processing of X-ray diffraction data collected in oscillation mode, *Methods Enzymol. 276*, 307−325.
19. Matthews, B. W. (1968) Solvent content of protein crystals, *J. Mol. Biol. 33*, 491−497.
20. Navaza, J. (2001) AmoRe: an automated package for molecular replacement, *Acta Crystallogr. D57*, 1367−1372.
21. Collaborative Computational Project, Number 4 (1994) *Acta Crystallogr. D50*, 760−763.
22. Zanotti, G., Scapin, G., Spadon, P., Veerkamp, J. H., and Sacchettini, J. C.(1992) Three-dimensional structure of recombinant human muscle fatty acid-binding protein, *J. Biol. Chem. 267*, 18541.
23. McRee, D. E. (1999) XtalView/Xfit: A versatile program for manipulating atomic coordinates and electron density, *J. Struct. Biol. 125*, 156−165.
24. Murshudov, G. N., Vagin, A. A., and Dodson, E. J. (1997) Refinement of the macromolecular structures by the maximum-likelihood method, *Acta Crystallogr. D54*, 1285−1294.
25. Laskowsky, R. A., MacArthur, M. W., Moss, D. S., and Thorntorn, J. (1993) PROCHECK: a program to check the stereochemical quality of protein structures, *J. Appl. Crystallogr. 26*, 283−291
26. Liang, J., Edelsbrunner, H., and Woodward, C. (1998) Anatomy of Protein Pockets and Cavities: Measurement of Binding Site Geometry and Implications for Ligand Design, *Protein Sci. 7*, 1884−1897.
27. Kirk, R. W., Kurian, E., and Prendergast, F. G. (1996) Characterization of the sources of protein-ligand affinity: 1-sulfonato-

8-anilinonaphthalene binding to intestinal fatty acid binding protein, *Biophys. J. 70*, 69−83.
28. Richieri, G. V., Ogata, R. T., and Kleinfeld A. M. (1992) A fluorescently labeled intestinal fatty acid binding protein, *J. Biol. Chem. 267*, 23495−23501.
29. Sacchettini, J. C., Gordon, J. I., and Banaszak, L. J. (1989) Crystal structure of rat intestinal fatty acid binding protein. Refinement and analysis of the *Escherichia coli*-derived protein with bound palmitate, *J. Mol. Biol. 208*, 327−339.
30. Eads, J., Sacchettini, J. C., Kromminga, A., and Gordon, J. I. (1993) Escherichia coli-derived rat intestinal fatty acid binding protein with bound myristate at 1.5Å resolution and I-FABP Arg106→Gln with bound oleate at 1.74Å resolution, *J. Biol. Chem. 268*, 26375−26385.
31. Herr, F. H., Aronson, J., and Storch, J. (1996) Role of the portal lysine residues in electrostatic interactions between heart fatty acid binding protein and phospholipid membranes, *Biochemistry 35*, 11840−11845.
32. Kennedy, M. W., Scott, J. C, Lo, S., Beauchamp, J., and McManus, D. P. (2000) Sj-FABPc fatty-acid binding protein of the human blood fluke Schistosoma japonicum: structural and functional characterization and unusual solvent exposure of a portal-proximal tryptophan residue, *Biochem. J. 349*, 377−384.
33. Vilar, M. M., Barrientos, F., Almeida, M., Thaumaturgo, N., Simpson, A., Garratt, R., and Tendler, M. (2003) An experimental bivalent peptide vaccine against schistosomiasis and fascioliasis, *Vaccine 22*, 137−144.
34. Ramos, C. R., Figueredo, R. C., Pertinhez, T. A., Vilar, M. M., do Nascimento, A. L., Tendler, M., Raw, I., Spisni, A., and Ho, P. L. (2003) Gene structure and M20T polymorphism of the *Schistosoma mansoni* Sm14 fatty acid binding protein, *J. Biol. Chem. 278*, 12745−12751.
35. Richieri, G. V., Low, P. J., Ogata, R. T., and Kleinfeld, A. M. (1998) Thermodynamics of fatty acid binding protein to engineered mutants of the adipocyte and intestinal fatty acid binding proteins, *J. Biol. Chem. 273*, 7397−7405.
36. Balendiran, K. G., Schnutgen, F., Scapin, G., Borchers, T., Xhong, N., Lim, K., Godbout, R., Spener, F., and Sacchettini, J. (2000) Crystal structure and thermodynamic analysis of human brain fatty acid binding protein, *J. Biol. Chem. 275*, 27045−27054
37. Hodson, M. E., and Cistola D. P. (1997) Ligand binding alters the backbone mobility of intestinal fatty acid binding protein by ^{15}N NMR relaxtion and ^{1}H exchange, *Biochemistry 36*, 2278−2290.
38. Kurian, E., Kirk, W. R., and Prendergast, F. G. (1996) Affinity for rRat intestinal fatty acid binding protein: Further examination, *Biochemistry 35*, 3865−3874.
39. Ory, J. J., and Banaszak, L. J. (1999) Studies of ligand binding reaction of adipocyte lipid binding protein using the fluorescent probe 1,8-anilinonaphthalene-8-sulfonate, *Biophys. J. 77*, 1107−1116.
40. Alvite, G., Di Pietro, S. M., Santomè, J. A., Ehrlich, R., and Esteves, A. (2001) Binding properties of *Echinococcus granulosus* fatty acid binding protein, *Biochim. Biophys. Acta 1533*, 293−302.
41. Esteves, A., Joseph, L., Paulino, M., and Ehrlich, R. (1997) Remarks on the philogeny and structure of fatty acid binding proteins from parasitic platyhelminths, *Int. J. Parasitol. 27*, 1013−1027.
42. LaLonde, J. M., Levenson, M. A., Roe, J. J., Bernlohr, D. A., and Banaszak, L. J. (1994) Adipocyte lipid-binding protein complexed with arachidonic acid, *J. Biol. Chem. 269*, 25339−25347.
43. Wootan, M. G., Bernlohr, D. A., and Storch, J. (1993) Mechanism of fluorescent fatty acid transfer from adipocyte fatty acid binding protein to membranes, *Biochemistry 32*, 8622−8627.
44. Eastman, S. J., Wilschut, J., Cullis, P. R., and Hope, M. J. (1989) Intervesicular exchange of lipids with weak acid and weak base characteristic: influence of transmembrane pH gradients, *Biochim. Biophys. Acta 981*, 178−184.
45. Richieri, G. V., and Kleinfeld, A. M. (1995) Unbound free fatty acid levels in human serum, *J. Lipid Res. 36*, 229−240.
46. Fan, J., Gan. J., Yang, W., Liying, S., McManus, D., and Brindley, P. J. (2003) A *Schistosoma japonicum* very low-density lipoprotein-binding protein, *Int. J. Biochem. Cell Biol. 35*, 1436−1451.

BI048505F